JACS
JOURNAL OF THE AMERICAN CHEMICAL SOCIETY

Article

pubs.acs.org/JACS

Photocatalytic Activity Enhanced by Plasmonic Resonant Energy Transfer from Metal to Semiconductor

Scott K. Cushing,[†,‡,§] Jiangtian Li,[‡,§] Fanke Meng,[‡] Tess R. Senty,[†] Savan Suri,[‡] Mingjia Zhi,[‡] Ming Li,[‡] Alan D. Bristow,[†] and Nianqiang Wu*[,‡]

[†]Department of Physics, West Virginia University, Morgantown, West Virginia 26506-6315, United States

[‡]Department of Mechanical and Aerospace Engineering, West Virginia University, Morgantown, West Virginia 26506-6106, United States

Supporting Information

ABSTRACT: Plasmonic metal nanostructures have been incorporated into semiconductors to enhance the solar-light harvesting and the energy-conversion efficiency. So far the mechanism of energy transfer from the plasmonic metal to semiconductors remains unclear. Herein the underlying plasmonic energy-transfer mechanism is unambiguously determined in Au@SiO_2@Cu_2O sandwich nanostructures by transient-absorption and photocatalysis action spectrum measurement. The gold core converts the energy of incident photons into localized surface plasmon resonance oscillations and transfers the plasmonic energy to the Cu_2O semiconductor shell via resonant energy transfer (RET). RET generates electron−hole pairs in the semiconductor by the dipole−dipole interaction between the plasmonic metal (donor) and semiconductor (acceptor), which greatly enhances the visible-light photocatalytic activity as compared to the semiconductor alone. RET from a plasmonic metal to a semiconductor is a viable and efficient mechanism that can be used to guide the design of photocatalysts, photovoltaics, and other optoelectronic devices.

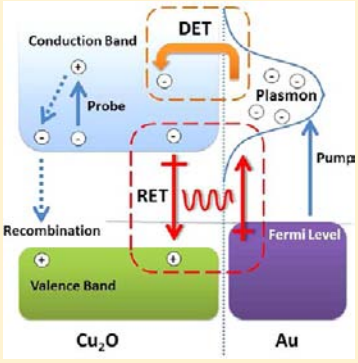

INTRODUCTION

Solar energy is a clean and abundant energy source that can be converted to electricity in photovoltaic devices, chemical energy by photocatalysts, and thermal energy using solar concentrators. The efficiency of solar conversion in photovoltaic and photocatalytic devices depends on four processes: light absorption, charge separation, charge migration, and charge recombination.[1,2] Semiconductors used in photovoltaic and photocatalytic devices have low solar-energy-conversion efficiency due to limitations in one or more of these four processes. For example, many commonly used semiconductors such as anatase TiO_2 and perovskite $La_2Ti_2O_7$ absorb only ultraviolet light,[3−6] which accounts for less than 5% of total solar radiation.

The recent and rapid development of surface plasmon resonance (SPR) has offered a new opportunity to overcome the limited efficiency of photocatalysts and photovoltaic devices. Incorporating plasmonic metal nanostructures into semiconductors can increase the efficiency of photovoltaic devices by 10−15%[7−18] and enhances photocatalytic activity toward organic compound decomposition[19−26] and water splitting.[27−29] SPR improves the solar-energy-conversion efficiency by (i) extending light absorption to longer wavelengths, (ii) increasing light scattering, and (iii) exciting electron−hole pairs in the semiconductor by transferring the plasmonic energy from the metal to the semiconductor.

Process (i) enables enhanced absorption of solar light in the semiconductor throughout the visible to near-infrared light range. This process concentrates the incident photon energy in plasmon oscillations. Process (ii) originates from the large scattering cross-section associated with SPR. Metallic nanoparticles will scatter incident light and locally amplify the electromagnetic field when placed on the surface or inside a solar material/device.[8,9] This results in an enhancement of the effective absorption cross section and an increase in the effective optical path length inside the semiconductor.

In process (iii), the concentrated energy contained in localized plasmonic oscillations is transferred to the semiconductor, inducing charge separation in the semiconductor. So far, the SPR-induced charge separation mechanism remains unclear. It has been reported that direct electron transfer (DET) occurs from the plasmonic metal to the conduction band of the semiconductor when they are in direct contact (Figure 1c) .[20,21,31−33] DET depends on the alignment of the band levels of the semiconductor and Fermi level of the plasmonic metal, so it is possible for electrons or holes to be transferred from the metal into the semiconductor at energies below the band gap if the electronic energy levels match. DET occurs after the excitation and subsequent decoherence of the SPR, which leaves a population of hot electrons that are able to undergo transfer to the semiconductor. For example, SPR-mediated hot electrons have been confirmed to be injected from gold nanoparticles to the conduction band of TiO_2.[30]

Received: June 10, 2012
Published: August 14, 2012

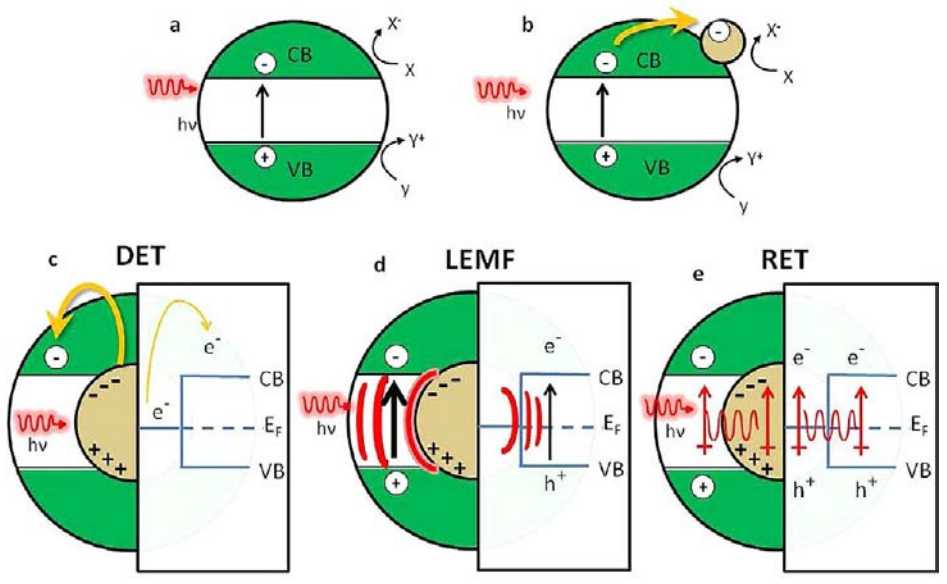

Figure 1. Charge separation mechanisms in various photocatalytic nanostructures. (a) Photoexcited ($h\nu$) semiconductors produce electrons (holes) in the conduction (valence) band [CB (VB)], each contributing to chemical reactions ($X + e^- = X^-$) and ($Y + h^+ = Y^+$) at their surface. (b) Metal nanoparticles can act as co-catalysts to provide additional surface sites via the trapping of electrons. Metal@semiconductor structures can increase charge separation by (c) direct electron transfer (DET) of hot electrons contained in LSPR to the semiconductor, (d) local electromagnetic field enhancement (LEMF) of the semiconductor charge separation process, and (e) resonant energy transfer (RET) from the LSPR dipole to the electron hole pair in the semiconductor shell.

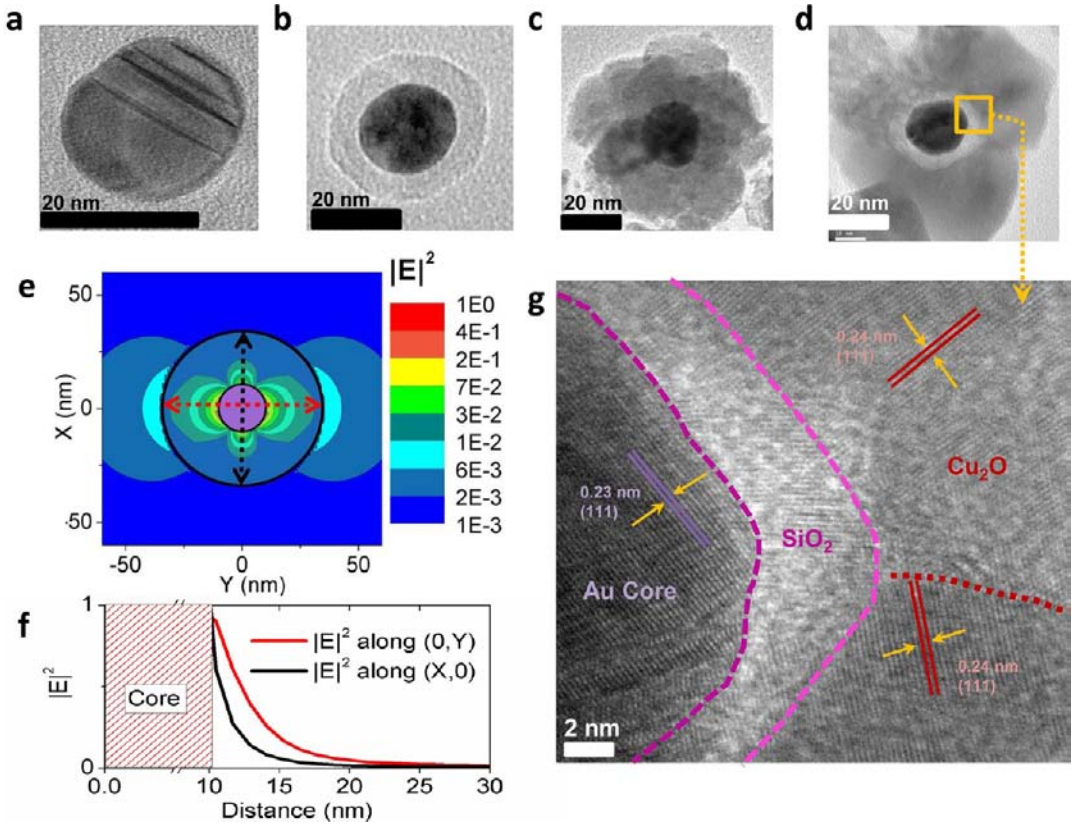

Figure 2. SEM images of the core-shell and sandwich nanoparticles. High-resolution transmission electron micrographs of (a) 20-nm uncoated Au nanosphere, (b) Au@SiO_2 core-shell structure, (c) Au@Cu_2O core-shell structure, and (d) Au@SiO_2@Cu_2O sandwich structure. The Cu_2O structure can be seen in Supplementary Figure S4. (g) An enlargement of the micrograph for the interface regions of the sandwich structure shows the various crystal orientations. (e) Discrete dipole approximation simulation of the local electromagnetic field created by the plasmonic core and extending into the surrounding Cu_2O shell for input radiation along the X axis, with (f) cross-sectional slices showing the EM field as a function of distance from the center of the Au core.

dx.doi.org/10.1021/ja305603t | J. Am. Chem. Soc. 2012, 134, 15033−15041

However; DET is not the only proposed mechanism. Recent studies have found that the photocatalysis of TiO_2 is still enhanced after an insulating interlayer is added between the metal and the semiconductor to prevent DET. It was proposed that the SPR-mediated local electromagnetic field (LEMF) radiatively contributed to the local generation of electron−hole pairs in the semiconductor (Figure 1d).[9,15,22,27,28,35,36] The LEMF-induced charge separation mechanism can create carriers only for energies above the band gap of the semiconductor.

In the present work, it is proposed that the electromagnetic field mediated plasmonic energy transfer can take the form of a resonant energy transfer (RET) process (Figure 1e). The RET process is proposed to be an alternative, nonradiative mechanism of SPR-induced charge separation in semiconductors. Whereas the radiative LEMF mechanism increases the rate of interband transitions in the semiconductor due to the increased local EM field, the RET process directly excites electron−hole pairs in the semiconductor nonradiatively through the relaxation of the localized surface plasmon dipole. Plasmon-induced RET in the near field is similar to Förster resonance energy transfer (FRET), where the LSPR dipole replaces the fluorescent system.

If RET can efficiently create electron−hole pairs in the semiconductor, it will broadly increase the scope of materials that can be enhanced by plasmonic energy transfer. DET can transfer charge carriers to the semiconductor at energies below band gap; however, DET material selection is limited by the electronic band structure alignment of the semiconductor and metal. In order for the plasmonic electrons to transfer into the conduction band of the semiconductor, charge equilibrium must be maintained, often necessitating the use of hole scavengers. The LEMF mechanism does not suffer from charge equilibration issues since the interband transition rate in the semiconductor is increased radiatively by the local field. However, the materials selection is still limited since LEMF cannot enhance charge separation at energies below the band gap. LEMF can only enhance the rate of the semiconductors interband transitions, not extend carrier creation to longer wavelengths. Like LEMF, the nonradiative dipole−dipole energy transfer of RET is not limited by electronic band structure matching and charge equilibration, since the energy of the plasmon transfers to an electron−hole pair in the semiconductor through a near field electromagnetic interaction. However, unlike previous reports of LEMF, it is demonstrated in this paper that RET can create electron−hole pairs in the semiconductor at energies both above and below the band gap due to nonradiative coupling with optically inaccessible and optically inefficient states at the band edge. RET can overcome the charge equilibration issues of DET while still enhancing carrier creation at energies below the band gap, unlike LEMF.

Previous studies on determining the SPR-enhanced photocatalysis mechanism have placed metal nanoparticles on the surface of semiconductors as a co-catalyst. The observed enhancement may be due to both plasmonic enhancement of the catalyst and/or simply self-catalysis of the co-catalyst. Other experiments have randomly dispersed metal nanoparticles into a semiconductor matrix, leading to a large variation in the SPR position and local electromagnetic field distribution, which affect the transfer mechanism. Unambiguously resolving the dominant energy transfer mechanism requires the design of controllable metal/semiconductor composite nanostructures.

To investigate the possibility of plasmonic energy transfer by RET, core-shell Au@Cu_2O (Figure 2c) and sandwiched Au@SiO_2@Cu_2O nanoparticles (Figure 2d) have been synthesized. These structures have been engineered to isolate the plasmonic energy transfer mechanisms as follows. Gold and Cu_2O are chosen due to the overlap between the localized surface plasmon resonance (LSPR) band of the Au core and the band gap absorption of Cu_2O, which allows for RET. Embedding the metal inside of the semiconductor eliminates possible self-catalysis effects of the metal (Figure 1b). The thin SiO_2 layer acts to electronically insulate the metal from the semiconductor while still allowing unattenuated propagation of the optical field around the nanoparticle.[14] The interlayer effectively blocks direct electron transfer (DET) between the Au and Cu_2O while still allowing for RET. In addition, significant light scattering and enhancements to the optical path length are only seen in large plasmonic metal nanoparticles (>50 nm).[41] The sandwich structure designed for this study utilizes a gold core that is only 20 nm in a diameter, eliminating enhancements due purely to increased scattering (process ii). The designed sandwich structure thus allows us to investigate how the plasmonic energy of the Au core is transferred to the semiconductor shell in the presence and absence of an insulating interlayer without the effects of light scattering and metal catalysis.

The present work uses a controlled structure, designed to isolate the electromagnetic field mediated plasmonic energy transfer mechanisms from the DET mechanism so that it can be determined if a RET process is responsible for the enhanced creation of carriers in the semiconductor. A combination of photocatalysis action spectrum, transient-absorption spectroscopy, and theoretical calculation shows for the first time that electron−hole pairs in the semiconductor are created via resonant energy transfer (RET) from the plasmonic metal (Figure 1e), which in the near field is similar to Förster resonance energy transfer (FRET). The RET process excites electron−hole pairs in the semiconductor through the relaxation of the localized surface plasmon dipole. The radiative coupling component originally proposed in LEMF is not seen in our experiments, rather the electromagnetic field interaction is dominated in the near field by the nonradiative RET. The RET process is clearly distinguished from DET.

EXPERIMENTAL SECTION

Synthesis of Au Nanospheres and Au@SiO_2 Nanospheres. Au nanospheres were synthesized by reducing $HAuCl_4$ with sodium citrate according to the Frens method.[37] Four milliliters of 1 wt % sodium citrate was added to 200 mL of 5 mM $HAuCl_4$ solution at a boil. Silica was coated on the Au nanospheres using the sodium silicate hydrolyzing technique in basic solution.[38] Two hundred microliters of 2 mM aminopropyltrimethoxysilane (APS) was added into 20 mL of the Au colloids and stirred for 30 min followed by 500 μL of 0.54 wt % sodium silicate and 30 min stirring. Finally 20 mL of ethanol was added and the mixture stood for 2 days.

Synthesis of Au@Cu_2O Core-Shell Nanoparticles and Au@SiO_2@Cu_2O Sandwich Nanoparticles. The Au@Cu_2O core-shell nanoparticles were synthesized following a previously reported procedure. Two milliliters of the as-prepared Au colloids was added to the solution containing 0.1 M $CuCl_2$ and 0.0338 M sodium dodecyl sulfate (SDS). Next 0.25 mL of 1 M NaOH and 0.45 mL of 0.2 M NH_4OH·HCl were added with stirring. The synthesis procedure for the Au@SiO_2@Cu_2O sandwich nanoparticles was the same as the Au@Cu_2O except that the Au colloids were replaced with Au@SiO_2 colloids.

Characterization. The nanoparticles were observed using a JEOL 7600F field emission scanning electron microscope. X-ray photo-

dx.doi.org/10.1021/ja305603t | J. Am. Chem. Soc. 2012, 134, 15033−15041

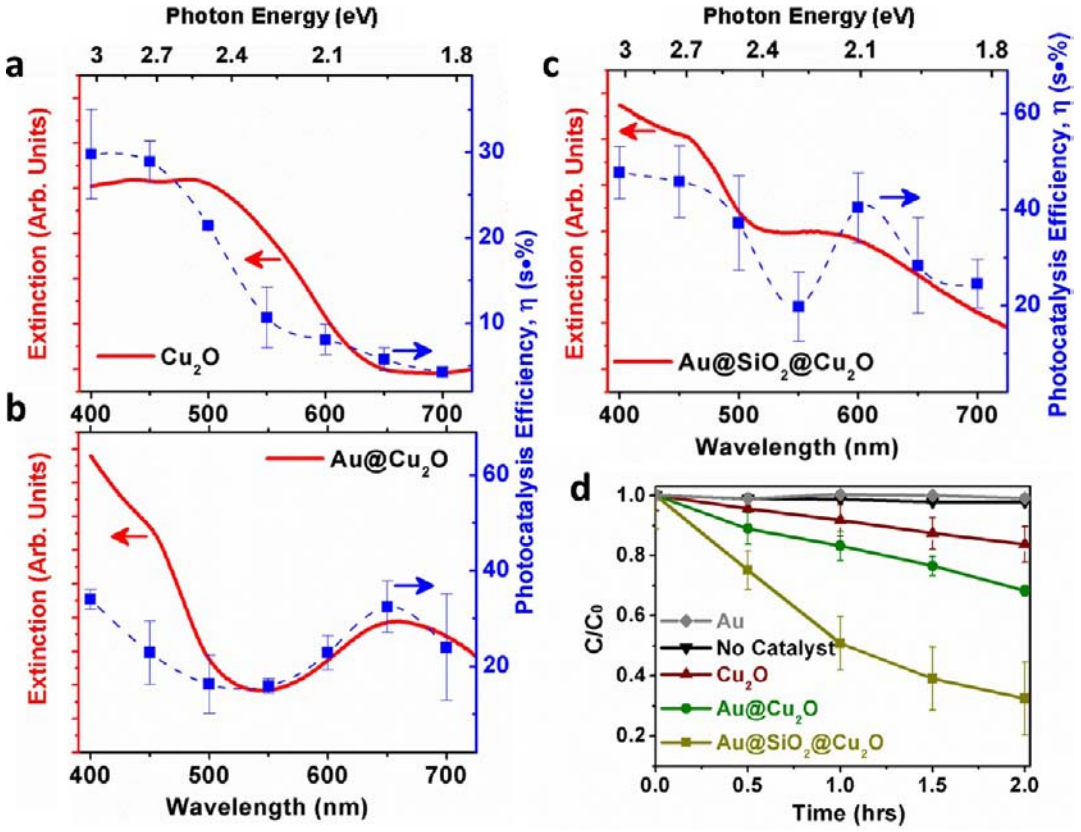

Figure 3. Ultraviolet−visible spectra and photocatalytic action spectra for (a) Cu_2O, (b) Au@Cu_2O, and (c) Au@SiO_2@Cu_2O. (d) Visible-light photodegradation of methyl orange versus time is monitored for no catalyst, uncoated Au, Cu_2O control, Au@Cu_2O, and Au@SiO_2@Cu_2O nanostructures.

electron spectroscopy was performed using a PHI 5000 Versa Probe. Exctinction was measured using a Shimadzu 2550 spectrometer.

Measurement of Photocatalytic Activity under Visible and Monochromatic Light Irradiation. The photocatalytic activity was evaluated by the degradation of methyl orange. A photoreactor equipped with fourteen 8 W visible light lamps (Cool white Fluorescent, range from 400 to 700 nm) was used as the light source. Photocatalysts at 0.15 mg/mL were dispersed in 40 mL of 50 mg/L methyl orange and allowed to reach adsorption/desorption equilibrium. The residual amount of MO at various times was determined using a Shimadzu spectrophotometer. The same procedure was followed for the wavelength-dependent photocatalytic activity except the light source was a 300 W Xe lamp coupled to a monochromator.

Transient Absorption. Non-degenerate pump−probe experiments were performed with 100-fs pulses from a 1 kHz Ti:sapphire laser amplifier (Libra) and an optical parametric amplifier (OPerA Solo). Pump pulses from the OPerA Solo where doubled in a β-barium borate crystal to provide a tunable wavelength source from 620 to 750 nm. Probe pulses were taken directly from the Libra. Time-delay between the pulses was controlled by a motion control system with a 4-ns time range. Focused beam spot sizes were 400 μm for the pump and 240 μm for the probe. Samples were dispersed in a KBr matrix. Transmission probe radiation was collected on a photodetector and recorded with a lock-in amplifier.

Discrete Dipole Approximation Simulations. Simulations of the local electromagnetic field were performed using the free program DDSCAT.[39] The refractive index for Cu_2O and Au was taken from Palik[40] and the online Sopra N and K database. The input source was 656 nm and linearly polarized along the X axis.

RESULTS AND DISCUSSION

a. Structures of Photocatalysts. The high-resolution transmission electron micrographs (HRTEM) in Figure 2 show the result of the synthesis of the core-shell and sandwich nanostructures. First 20-nm diameter Au nanospheres were synthesized (Figure 2a), which were then coated with a ∼5 nm thick SiO_2 layer to form a Au@SiO_2 core-shell structure (Figure 2b and Supplementary Figure S1 in Supporting Information) and a ∼25 nm thick Cu_2O layer to form a Au@Cu_2O core-shell nanoparticles (Figure 2c and Supplementary Figure S2). The former core-shells were coated with a ∼25-nm thick Cu_2O layer to create a Au@SiO_2@Cu_2O structure (Figure 2d,g). From the HRTEMs, the (111) planes of the single-crystalline Au cores were visible, and SiO_2 was observed to be amorphous. The Cu_2O shells were polycrystalline, regardless of being coated directly on the Au core or the SiO_2 layer. The chemical composition of the Au cores and the Cu_2O shells was confirmed by X-ray photoelectron spectroscopy (Supplementary Figure S3). Cu_2O particles were also synthesized for comparison of optical and photochemical properties (Supplementary Figure S4).

b. Light Absorption and Photocatalytic Activity. Figure 3 shows UV−vis extinction spectra for the Cu_2O, Au@Cu_2O, and Au@SiO_2@Cu_2O nanoparticles dispersed in the aqueous solutions. Bare gold nanospheres exhibited a broad LSPR centered at 520 nm (Supplementary Figure S5). Coating the Au nanospheres with the SiO_2 layer resulted in a red-shift of the plasmon peak to 525 nm (Supplementary Figure S5). Pure Cu_2O samples showed interband absorption, which was cut off at about 620 nm (Figure 3a). For Au@Cu_2O core-shell nanoparticles, the LSPR shifted to 650 nm (Figure 3b) due to an increase in the contrast of the effective dielectric constant between the core and cladding.[34] Similarly, the Au@SiO_2@

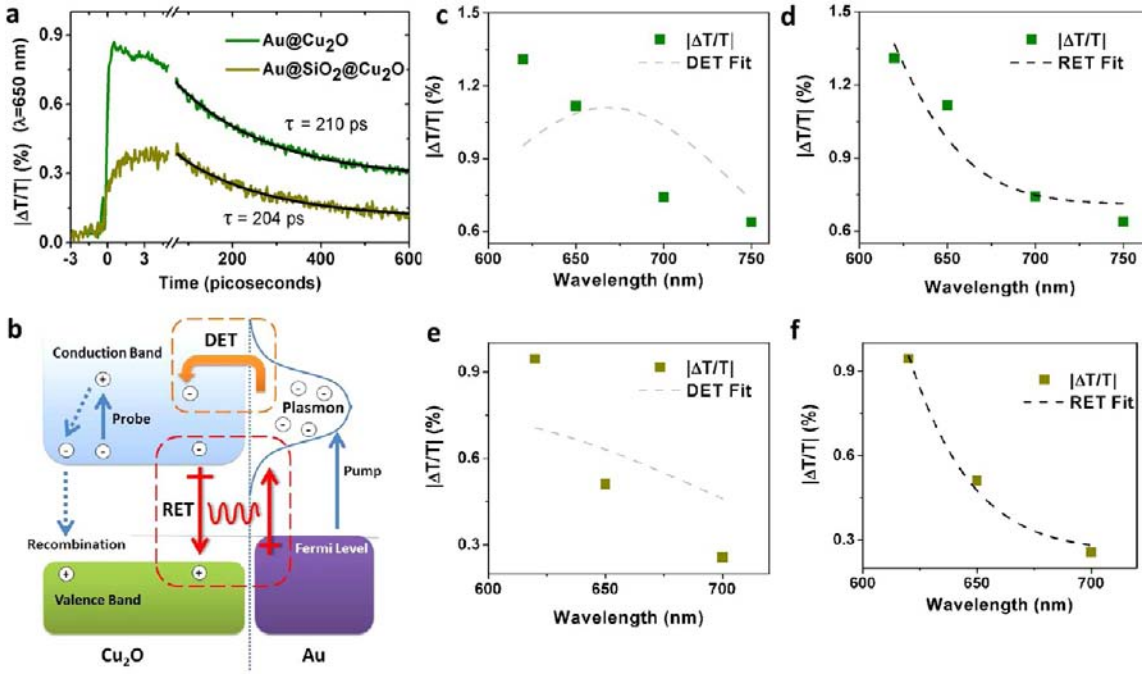

Figure 4. Ultrafast pump−probe measurements for core-shell and sandwich structures. (a) Transient absorption for Au@Cu_2O and Au@SiO_2@Cu_2O nanostructures acquired with a wavelength of 650 nm and a laser fluence of 7 mJ/cm^2. Decays are fit showing nearly identical recombination rates. (b) Schematic representation of the various transfer mechanisms that can occur in the Au@Cu_2O structure. Also shown in the diagram are the pump, probe (free-carrier absorption), and recombination paths. Wavelength-dependent signal amplitudes for Au@Cu_2O nanoparticles are fit with (c) DET and (d) RET models. Similarly, (e) DET and (f) RET models are applied to experimental data from the Au@SiO_2@Cu_2O nanoparticles.

Cu_2O sandwich structure showed a shifted LSPR at 600 nm (Figure 3c) due to a change in the dielectric contrast. At wavelengths below 500 nm, increased scattering increased the extinction for both the core-shell and sandwich nanoparticles. The colors of the four types of nanoparticle suspensions under visible-light radiation were consistent with the results of the UV−vis absorption spectra (Supplementary Figure S6). The local electromagnetic field associated with the plasmon resonance was determined by discrete dipole approximation simulations assuming perfect spherical symmetry (Figure 2e,f). The extent of the field confirms that the near field can interact with the semiconductor enhancing charge separation.[28,42−44] The local nature of the LSPR field suggests that if plasmon-mediated charge separation exists in the semiconductor, it will proceed through RET. Quadrupole moment terms are weak and can be neglected.

The photocatalytic activity of the Au@SiO_2@Cu_2O, Au@Cu_2O, and pure Cu_2O nanoparticles were evaluated by the photodegradation rate of methyl orange in the aqueous solution under visible-light irradiation (Figure 3d). The corresponding kinetic data is shown in Supplementary Figure S7. The Au@Cu_2O core-shell nanoparticle showed better photocatalytic activity compared with that of the pure Cu_2O nanoparticles (Figure 3d). The Au core was isolated from the reactant by the semiconductor shell, ruling out the chemical catalysis effect of the Au nanoparticles. The Au@SiO_2@Cu_2O sandwich nanoparticles exhibited the best photocatalytic activity among the three samples tested. It has been reported that LSPR-induced localized heating in the metal nanoparticles can lead to thermochemical degradation of the organic compounds.[21,42] To ensure the enhanced photocatalytic activity was not due to heating, the degradation of methyl orange was measured under visible-light irradiation in the presence of the bare Au nanospheres and the Au@SiO_2 nanoparticles (Supplementary Figure S8). The results showed that neither the bare Au nanospheres nor the Au@SiO_2 nanoparticles were able to thermally activate the decomposition of methyl orange under visible-light irradiation.

To determine whether the LSPR was responsible for enhancement of the photocatalytic activity, the extinction spectra of the nanoparticles were directly compared to the action spectra of apparent photocatalysis efficiency (Figure 3a−c). The apparent photocatalysis efficiency per unit time is defined as $\eta = [1240\ \text{eV nm}[(C_0 - C)/C_0)]/[P\lambda]$ where P is the power density of the monochromatic light in W, and λ is the wavelength in nm. C_0 and C are the initial and final concentrations of reactant in mol/L after a certain irradiation time, respectively. The apparent photocatalysis efficiency was defined to normalize the photocatalysis by the differing power of monochromated light at each wavelength used in the action spectrum. It was not intended to reflect an absolute quantum yield for photocatalysis. The action spectra show the apparent photocatalysis efficiency as a function of the wavelength of incident monochromatic light. The pure Cu_2O nanoparticles exhibited photocatalytic activity that followed the extinction spectrum (Figure 3a), with negligible photocatalytic activity (efficiency) below the band edge. It should be noted that the photocatalysis was weak for excitation at 550 nm near the band edge of Cu_2O, which indicated that the absorption at the wavelength may be dominated by trap states that were inefficient for photocatalysis. The trend was consistent for the Cu_2O, Au@Cu_2O, and Au@SiO_2@Cu_2O nanoparticles, independent of the structure or the possible transfer mechanisms.

The photocatalysis action spectrum (Figure 3b) for the Au@Cu_2O nanoparticles also followed the trend of the extinction spectrum, showing significant enhancement at the LSPR

dx.doi.org/10.1021/ja305603t | J. Am. Chem. Soc. 2012, 134, 15033−15041

wavelengths as compared to pure Cu_2O. This enhancement can happen only if light excited the plasmon and then energy or charge was transferred to the semiconductor to drive the photocatalysis. While it is likely that RET mediates the energy transfer from plasmon to semiconductor because of the overlap of the LSPR and the Cu_2O conduction band, the electromagnetic interaction mechanism cannot be separated from DET using the Au@Cu_2O photocatalysis data alone. Only the involvement of the LSPR in creating charge separation can be proven from the Au@Cu_2O nanoparticles.

The photocatalysis action spectrum of the Au@SiO_2@Cu_2O sandwich nanoparticles was examined to determine whether the DET or RET mechanism was dominant. Once again the action spectrum generally followed the extinction spectrum (Figure 3c), with strong enhancement as compared to pure Cu_2O. DET was suppressed due to the insulating silica layer that acted as a barrier for electron transfer. The enhanced photocatalytic activity at the LSPR wavelengths must therefore be due to an interaction between the LSPR and semiconductor through the local electromagnetic field. RET is the most probable near-field interaction mechanism due to coupling of the large plasmonic dipole moment to the electron−hole pair dipole moment in the semiconductor shell. The relaxation of the LSPR dipole will lead to the excitation of electron−hole pairs in the semiconductor resulting in enhanced photocatalysis. The relative strength of the energy transfer depends on the overlap integral of the plasmon resonance and the conduction band (eq 3 in Supporting Information). Details of extracting the overlap integral are discussed later, but the overlaps are shown in Supplementary Figures S12 and S13 for the core-shell and sandwich structures. Since the Au@SiO_2@Cu_2O structure had the largest overlap integral, it should show the highest photocatalytic efficiency according to the RET theory. This initial comparison agrees with the theory of RET and is supported by the fast photodegeneration observed in the Au@SiO_2@Cu_2O under white-light illumination (Figure 3d).

c. Transient-Absorption Spectroscopy. Photocatalysis spectra are a result of carriers that have reached the surface of the Cu_2O nanoparticle and contribute to the photodegradation of the reactant. The photocatalysis spectra do not directly show how the carriers are created. Both RET and DET can create carriers in the trap and defect states in Cu_2O, which may be inefficient in photocatalysis, such as the states present at 550 nm, distorting the spectral efficiency seen in the action spectrum measurements. To further investigate the plasmon-mediated energy-transfer mechanism, transient-absorption spectroscopy was performed on the Au@Cu_2O core-shell and the Au@SiO_2@Cu_2O nanoparticles to monitor the carrier dynamics and relaxation times (Figure 4). In these pump−probe measurements, the samples were dried films, and 100-fs pulses excite the plasmon and probe the carriers created in the conduction band of the Cu_2O respectively. Pump pulses were varied in wavelength from 620 to 750 nm (Supplementary Figures S10 and S11) across the plasmon resonances and in fluence from 7 to 15 mJ/cm^2. Carriers created in the Cu_2O by plasmonic energy transfer were probed by an 800-nm pulse that transmits through the sample. Because the probe wavelength is longer than the wavelengths required for interband absorption or for plasmon excitation, the signal is due to free-carrier absorption in the conduction band of the Cu_2O only. Since Cu_2O is usually a p-type semiconductor, the transient absorption at 800 nm may include a contribution due to excited electrons or holes. However, to determine the energy transfer mechanism, only the relative number of electron hole pairs verse the wavelength is necessary, not the identity of the carriers probed. Hence, the relative change in transmission $|\Delta T/T|$ was directly proportional to the relative number of carriers created in the Cu_2O by plasmonic energy transfer. Contributions to $|\Delta T/T|$ from the Au were excluded on the basis of short time-scale and low-amplitude response in transient absorption measurements performed on the uncoated cores.[45] Typical transients for the core-shell and sandwich nanostructures are shown in Figure 4a, excited at 650 nm and low fluence. This wavelength was not at the peak of either plasmon resonance but was further off resonance for the Au@SiO_2@Cu_2O, resulting in the lower signal amplitude.

The rise time of the signals from the Au@Cu_2O has fast (<100 fs) and slow (~2 ps) components, where the result of the fast excitation began to decay before the slower contribution had concluded. The fast component is most likely due to direct interactions in the metal. For Au@SiO_2@Cu_2O, only the slower rise component survives due to a simpler energy transfer scheme as might be expected by inserting the insulating layer into the structure. Carriers created in the Cu_2O for both core-shell and sandwich structures were observed to have lifetimes on the order of a few hundred picoseconds, which was consistent with interband recombination. As the time delay is increased, the population of free carriers that contribute to absorption decrease due to this recombination. The difference in the decay for the two samples was on the order of a few percent, which was only just outside the reproducibility of the experiment. These slight differences in the recombination time may arise from a nonradiative relaxation mechanism through the metal for the Au@Cu_2O nanoparticles.[22]

Plasmon-induced charge separation mechanisms are illustrated in Figure 4b (DET and RET). RET describes the nonradiative transfer of energy by dipole−dipole interactions. The interaction strength depends on the separation distance between the dipoles and the overlap integral of the interacting dipoles' spectra (eq 3 in Supporting Information). RET and DET can be differentiated by the wavelength- and fluence-dependent carrier density, which is proportional to $|\Delta T/T|$. To ensure that $|\Delta T/T|$ maps only the transferred carrier-density the signal was extracted at a time delay between the pump and probe of ~10−15 ps (Supplementary Figures S10 and S11). In this time window all fast coherent dynamics, thermalization, and Au signatures have occurred and recombination has not measurably decreased the contributing carrier density. Wavelength-dependent $|\Delta T/T|$ for Au@Cu_2O (Figure 4c,d) and Au@SiO_2@Cu_2O (Figure 4e,f) nanoparticles were compared to DET and RET theory. Fluence dependence is shown in Supplementary Figure S14.

The excited plasmon produces a Gaussian distribution of hot electrons, which are able to transfer to the semiconductor.[19,20,30−32] If DET is the dominant plasmonic energy transfer mechanism, then the wavelength-dependent excited carrier density in the semiconductor will follow the line shape of the plasmon absorption.[33,50] To test DET theory, first the appropriate Gaussian line shape (Supplementary Figure S12) was obtained from the extinction spectrum (Figure 3b). A wavelength- and fluence-dependent surface was constructed from the Gaussian and assuming a linear dependence on fluence. The surface was used to fit the experimental data, leaving only the Gaussian amplitude and the slope of the fluence-dependence as free parameters. As can be seen from

Figure 4c and Supplementary Figure S14a, the DET surface does not agree well with the experimental data, indicating that DET is not the correct transfer mechanism.

If RET is the dominant mechanism, the number of carriers created in the semiconductor conduction band obeys the dipole−dipole interactions for two distributions of dipoles.[46,47] Hence, the generated carriers will follow the overlap integral[48−50] between the plasmon and the Cu_2O density of states (eq 3 in Supporting Information). A fitting procedure similar to that used for DET was applied to the RET mechanism, such that the Gaussian representing the plasmon is replaced by the overlap function (Supplementary Figure S12) and then used to create a wavelength- and fluence-dependent surface. Only the slope of the fluence-dependence and amplitude of the overlap integral were free parameters in the fit. In contrast to the DET surface, the RET surface fit (Figure 4d and Supplementary Figure S14b) had excellent agreement to the experimental data, indicating that RET is the dominant mechanism for energy transfer from plasmonic Au to Cu_2O.

To verify the findings of RET as the mechanism for solar energy conversion from the plasmonic metal to the semiconductor conduction band, wavelength- and fluence-dependence tests were also performed on the $Au@SiO_2@Cu_2O$ sandwich nanostructure. In these structures the 5-nm thick SiO_2 layer prevented DET. Note that if electron tunneling is present the signature would be clearly visible in the wavelength dependence. Hence, the only contribution should be RET, which is consistent with the simpler ∼2 ps rise in $|\Delta T/T|$. As for the $Au@SiO_2@Cu_2O$ sandwich samples, the wavelength- and fluence-dependent carrier density was extracted from the transient absorption and compared to surfaces for DET (Figure 4e and Supplementary Figure 14c) and RET (Figure 4f and Supplementary Figure S14d). The Gaussian distributions representing the plasmon resonance for DET and the overlap integral for RET were extracted from the extinction (Supplementary Figure S13). In modeling, the fluence-dependent slope and the amplitudes of the various distributions remained the only free parameters. Once again, the RET model shows excellent agreement with the experimental results and the DET model does not, proving that RET is the dominant energy transfer mechanism for the $Au@SiO_2@Cu_2O$ nanostructures.

d. Theoretical Calculation. The transient-absorption and photocatalysis data show that the LSPR dipole creates electron−hole pairs in the semiconductor by RET. In particular, the overlap between the LSPR of the Au core and the interband absorption of Cu_2O are well matched to demonstrate the RET process. To validate this conclusion and examine the exact form of the interaction term, the transition rate was theoretically calculated using Fermi's golden rule. The final form of the calculation shows the dominant electromagnetic field mediated interaction between the semiconductor and LSPR is RET, similar in the short-range asymptote to FRET. The full calculation is outlined in the Supporting Information, but it can be summarized as follows.

The interaction of the semiconductor with the electromagnetic field near the valence band edge can be treated in the dipole approximation. It can be shown from the semiclassical light−matter interaction Hamiltonian that Bloch wave eigenstates are perturbed due to the electromagnetic field:[51]

$$H' = \frac{e}{2mc}(\vec{A}\cdot\vec{p}) \tag{1}$$

Through the commutator of position and momentum, H' is equivalent to the dipole-field interaction Hamiltonian:[52]

$$H' = -\vec{\mu} \bullet \vec{E} \tag{2}$$

Hence, near the band edge, absorption in the semiconductor can be approximated by the interaction of a dipole-matrix element μ with the local electromagnetic field E. In the case of the sandwich nanoparticles, the semiconductor experiences an electromagnetic field composed of the incident radiation, E_0, and the dipole field of the LSPR, E_{LSPR}. The dipole moment of the LSPR can be calculated from Mie theory as[53]

$$\mu_{LSPR} = \frac{\varepsilon_{metal} - \varepsilon_{dielectric}}{\varepsilon_{metal} + 2\varepsilon_{dielectric}} a^3 E_0 \tag{3}$$

where ε is the dielectric constant and a is the metal nanoparticle radius. By inserting the electric dipole field of the LSPR into the light−matter interaction Hamiltonian for the semiconductor, the dipole−dipole interaction Hamiltonian is recovered, which leads to the familiar RET equation in agreement with the experimental data.

It has been proposed in previous reports that the LEMF mechanism responsible for plasmon mediated charge separation could be a radiative or nonradiative interaction. The theoretical calculations and experimental data presented in this work indicate the LEMF mechanism is solely RET, a nonradiative process. Quantum electrodynamics can be used to calculate the full interaction Hamiltonian between the dipole LSPR field and the dipole distribution in the semiconductor to determine if a radiative contribution is also present. A full quantum electrodynamics (QED) theory for the interaction of two dipoles by the electromagnetic field[54] can be summarized in terms of the total transition rate, which is composed of a RET transition rate, a far-field correction rate, and a radiative decay rate:

$$w_{total} = w_{RET} + w_{int} + w_{radiative} \tag{4}$$

where

$$w_{RET} = \frac{9\kappa^2 c^4}{8\pi\tau_{A*} n^4 r^6} \int F_A(\omega)\sigma_B(\omega)\frac{d\omega}{\omega^4} \tag{5}$$

$$w_{int} = \frac{9c^4}{8\pi\tau_{A*} n^2 r^4}(\kappa_3{}^2 - \kappa_1\kappa_3) \int F_A(\omega)\sigma_B(\omega)\frac{d\omega}{\omega^2} \tag{6}$$

and

$$w_{radiative} = \frac{9c^4\kappa_1{}^2}{8\pi\tau_{A*} r^2} \int F_A(\omega)\sigma_B(\omega)d\omega \tag{7}$$

$F_A(\omega)$ is the normalized fluorescence, $\sigma_B(\omega)$ is the absorption coefficient, c is the speed of light, n is the refractive index, κ is an orientational factor as outlined in the Supporting Information, r is the distance between the two dipoles, and τ_{A*} is the radiative lifetime of F_A. In the near field, the full QED treatment is identical to the expression derived using Fermi's golden rule and the dipole−dipole interaction Hamiltonian for RET.[54] No other near field terms arise from the calculation, so the plasmon mediated interaction mechanism must be the nonradiative RET and not a radiative term proportional to $|E_{LSPR}/E_0|^2$. This is in agreement with the transient-absorption and photocatalysis measurements.

The enhancement of the transition probability due to the RET mechanism compared to the incident radiation E_0 can be

estimated by calculating the value of $\sigma_B(\omega)$ and $F_A(\omega)$. The transition rate for the semiconductor, which is directly proportional to the absorption coefficient, is found using Fermi's golden rule and summing over all possible states assuming only direct transitions and a parabolic band gap[51]

$$w_{semi} = \frac{e^2 |E_0|^2}{4\pi^2 m^2 \hbar\omega^2} |p_0|^2 \left(\frac{2m_{reduced}}{\hbar^2}\right)^{3/2} (\hbar\omega - E_g)^{1/2} \quad (8)$$

where m is the electron mass, $m_{reduced}$ is the reduced mass of the electron and hole, p_0 is the momentum matrix element in the semiconductor, and E_g is the band gap energy of the semiconductor in eV. The function $F_A(\omega)$ can be estimated by using the dipole moment of the LSPR from Mie theory (eq 3) and an area normalized Lorentzian $f(\omega)$.[53] The ratio between the probability of exciting an electron hole pair in the semiconductor by RET and by the incident field becomes

$$\frac{w_{RET}}{w_{semi}} = \frac{20\pi\kappa^2\hbar\omega^2}{n^5}\frac{a^6}{r^6}\left|\frac{\varepsilon_{metal} - \varepsilon_{die}}{\varepsilon_{metal} + 2\varepsilon_{die}}\right|^2 \frac{\int f(\omega)(\hbar\omega - E_g)^{1/2}\frac{d\omega}{\omega^2}}{(\hbar\omega - E_g)^{1/2}} \quad (9)$$

where the frequency dependence of ε and p_0 have been ignored as a first approximation. The above must be integrated over the distance of interaction r and the range of frequencies ω to see the full enhancement, but can be approximated by taking $r = a$ and evaluating the overlap integral numerically. Assuming a band gap of 600 nm and a LSPR centered at 600 nm with a half width of 100 nm for a gold nanoparticle (with ε_{metal} roughly negative $2\varepsilon_{dielectric}$ as required for LSPR), the enhancement is approximately 10,000. The large increase in transition probability allows optically inefficient band edge, surface, and defect states to effectively support photocatalysis. It has also been reported that the near-field interaction can allow indirect transitions and coupling to optically forbidden states.[55,56] These possible routes of coupling to below band edge states explain how in our study the RET mechanism can effectively extend the band gap of the semiconductor to lower energies.[15,22,27,28,35,36]

CONCLUSIONS

Förster resonance energy transfer (FRET) has been well studied in various systems such as organic dye−dye, quantum dot−quantum dot, dye−gold nanoparticle, and quantum dot−gold nanoparticle systems. Herein it is proven that the local electromagnetic field mediates energy transfer through RET from a plasmonic metal to a semiconductor, inducing charge separation in the semiconductor. Conventional FRET in a dye−dye system is a downward energy transfer process. In contrast, the newly discovered RET from a plasmonic metal to a semiconductor can be thought of as an effectively upward energy transfer process, allowing for the conversion of below band edge light into charge carriers in the semiconductor, as demonstrated in the present work. Of course energy is conserved, and it is the overlap between broad energy resonances that allow for the seemingly upward energy transition.

Hence, a plasmonic metal nanostructure can act as a photosensitizer via the RET process. A photosensitizer's ability to extend a semiconductor's effective optical band gap with conversion efficiency equal to that in wavelength below the band gap could transform design in photocatalysts, photovoltaic devices, and other optoelectronic devices. In addition, the light absorption of the plasmonic photosensitizer can be tuned from the visible-light to near-infrared wavelength range by tailoring the LSPR. Furthermore, RET from a plasmon resonance to a semiconductor does not require direct contact between the energy donor and acceptor. Given that the local electromagnetic field surrounding a plasmonic nanostructure can reach tens of nanometers, the resonance distance in RET from a plasmonic metal to a semiconductor could be longer than the typical Förster distance (R_0 = 6 nm in conventional FRET).

Semiconductors are often coupled with conventional photosensitizers such as organic dyes and inorganic quantum dots to enable light harvesting in the visible-light or near-infrared regime. Such coupling is based on the direct electron transfer from the conduction band of the photosensitizer to the conduction band of the semiconductor. In order for the electron transfer to be energetically favorable, the photosensitizer's conduction band must be higher in energy than the semiconductors. As well, to maintain charge equilibrium, the valence band of the photosensitizer must also be electronically aligned to allow hole transfer. These conditions on band alignment place strict limits on material selection for efficient photosensitizers. In contrast, plasmonic photosensitizers based on the RET from a plasmonic metal to a semiconductor do not require electronic band alignment, offering much more flexibility for designing solar energy materials and optoelectronic devices.

ASSOCIATED CONTENT

Supporting Information

Experimental details and Figures S1−S13. This material is available free of charge via the Internet at http://pubs.acs.org.

AUTHOR INFORMATION

Corresponding Author

nick.wu@mail.wvu.edu

Author Contributions

[§]These authors contributed equally to this work.

Notes

The authors declare no competing financial interest.

ACKNOWLEDGMENTS

This work was supported by the National Science Foundation (CBET-1233795) and NSF Graduate Research Fellowship under Grant No. (1102689). The resource and facilities used in this work were partially supported by Research Challenge Grant from the State of West Virginia (EPS08-01), NSF (EPS 1003907), and the West Virginia University Research Corporation and the West Virginia EPSCoR Office.

REFERENCES

(1) Green, M. A. *Prog. Photovoltaics* **2009**, *17*, 183−189.

(2) Wu, N. Q.; Wang, J.; Tafen, D.; Wang, H.; Zheng, J. G.; Lewis, J. P.; Liu, X.; Leonard, S. S.; Manivannan, A. *J. Am. Chem. Soc.* **2010**, *132*, 6679−6685.

(3) Tafen, D.; Wang, J.; Wu, N. Q.; Lewis, J. P. *Appl. Phys. Lett.* **2009**, *94*, 093101.

(4) Meng, F.; Hong, Z.; Arndt, J.; Li, M.; Zhi, M.; Yang, F.; Wu, N. Q. *Nano Res.* **2012**, *5*, 213−221.

(5) Li, M.; Zhou, S.; Zhang, Y.; Chen, G.; Hong, Z. *Appl. Surf. Sci.* **2008**, *254*, 3762−3766.

(6) Li, M.; Tang, P.; Hong, Z.; Wang, M. *Colloids Surf., A* **2008**, *318*, 285−290.

(7) Catchpole, K. R.; Polman, A. *Opt. Express* **2008**, *16*, 21793.

(8) Stuart, H. R.; Hall, D. G. *Appl. Phys. Lett.* **1998**, *73*, 3815.

(9) Atwater, H. A.; Polman, A. *Nat. Mater.* **2010**, *9*, 205−213.
(10) Murdoch, M.; Waterhouse, G. I. N.; Nadeem, M. A.; Metson, J. B.; Keane, M. A.; Howe, R. F.; LIorca, J.; Idriss, H. *Nat. Chem.* **2011**, *3*, 489−492.
(11) Linic, S.; Christopher, P.; Ingram, D. B. *Nat. Mater.* **2011**, *10*, 911−921.
(12) Jones, M. R.; Osberg, K. D.; Macfarlane, R. J.; Langille, M. R.; Mirkin, C. A. *Chem. Rev.* **2011**, *111*, 3736−3827.
(13) Ferry, V. E.; Sweatlock, L. A.; Pacifici, D.; Atwater, H. A. *Nano Lett.* **2008**, *8*, 4391−4397.
(14) Brown, M.; Suteewong, T.; Kumar, R. S.; D'Innocenzo, V.; Petrozza, A.; Lee, M. M.; Wiesner, U.; Snaith, H. J. *Nano Lett.* **2011**, *11*, 438−445.
(15) Standridge, S. D.; Schatz, G. C.; Hupp, J. T. *J. Am. Chem. Soc.* **2009**, *131*, 8407−8409.
(16) Standridge, S. D.; Schatz, G. C.; Hupp, J. T. *Langmuir* **2009**, *25*, 2596−2600.
(17) Haegglund, C.; Zaech, M.; Kasemo, B. *Appl. Phys. Lett.* **2008**, *92*, 013113.
(18) Aydin, K.; Ferry, V. E.; Briggs, R. M.; Atwater, H. A. *Nat. Commun.* **2011**, *2*, 517.
(19) Awazu, K.; Fujimaki, M.; Rockstuhl, C.; Tominaga, J.; Murakami, H.; Ohki, Y.; Yoshida, N.; Watanable, T. *J. Am. Chem. Soc.* **2008**, *130*, 1676−1680.
(20) Hu, C.; Peng, T.; Hu, X.; Nie, Y.; Zhou, X.; Qu, J.; He, H. *J. Am. Chem. Soc.* **2010**, *132*, 857−862.
(21) Christopher, P.; Ingram, D. B.; Linic, S. *J. Phys. Chem. C* **2010**, *114*, 9173−9177.
(22) Mahmoud, M. A.; Qian, W.; EI-Sayed, M. A. *Nano Lett.* **2011**, *11*, 3285−3289.
(23) Ide, Y.; Matsuoka, M.; Ogawa, M. *J. Am. Chem. Soc.* **2010**, *132*, 16762−16764.
(24) Zhang, Q.; Lima, D. Q.; Lee, I.; Zaera, F.; Chi, M.; Li, Y. *Angew. Chem., Int. Ed.* **2011**, *123*, 7226−7230.
(25) Naya, S.; Inoue, A.; Tada, H. *J. Am. Chem. Soc.* **2010**, *132*, 6292−6293.
(26) Wang, P.; Huang, B.; Zhang, X.; Qin, X.; Jin, H.; Dai, Y.; Wang, Z.; Wei, J.; Zhan, J.; Wang, S.; Wang, J.; Whangbo, M. *Chem.—Eur. J.* **2009**, *15*, 1821−1824.
(27) Liu, Z.; Hou, W.; Pavaskar, P.; Aykol, M.; Cronin, S. B. *Nano Lett.* **2011**, *11*, 1111−1116.
(28) Ingram, D. B.; Linic, S. *J. Am. Chem. Soc.* **2011**, *133*, 5202−5205.
(29) Thomann, I.; Pinaud, B. A.; Chen, Z.; Clemens, B. M.; Jaramillo, T. F.; Brongersma, M. L. *Nano Lett.* **2011**, *11*, 3440−3446.
(30) Furube, A.; Du, L.; Hara, K.; Katoh, R.; Tachiya, M. J. *Am. Chem. Soc.* **2007**, *129*, 14852−14853.
(31) Tian, Y.; Tatsuma, T. *Chem. Commun.* **2004**, 1810−1811.
(32) Kowalska, E.; Mahaney, O.; Abe, R.; Ohtani, B. *Phys. Chem. Chem. Phys.* **2010**, *12*, 2344.
(33) Mubeen, S.; Hernandez-Sosa, G.; Moses, D.; Lee., J.; Moskovits, M. *Nano Lett.* **2011**, *11*, 5548−5552.
(34) Kumar, M. K.; Krishnamoorthy, S.; Tan, L. K.; Chian, S. Y .; Tripathy, S.; Gao, H. *ACS Catal.* **2011**, *1*, 300−308.
(35) Wang, L.; Clavero, C.; Huba, Z.; Carroll, K. J.; Carpenter, E. E.; Gu, D.; Lukaszew, R. A. *Nano Lett.* **2011**, *11*, 1237.
(36) Tcherniak, A.; Ha, J. W.; Dominguez-Medina, S.; Slaughter, L. S.; Link, S. *Nano Lett.* **2010**, *10*, 1398−1404.
(37) Frens, G. *Nat. Phys. Sci.* **1973**, *241*, 20−22.
(38) Liz-Marzan, L. M.; Giersig, M.; Mulvaney, P. *Langmuir* **1996**, *12*, 4329−4335.
(39) Draine, B. T.; Flatau, P. J. *J. Opt. Soc. Am.* **1994**, *A11*, 1491−1499.
(40) Palik, E. D. *Handbook of Optical Constants of Solids*; Academic Press: Boston, 1985.
(41) Jain, P. K.; Huang, X.; EI-Sayed, I. H.; EI-Sayed, M. A. *Acc. Chem. Res.* **2008**, *41*, 1578−1586.
(42) Rycenga, M.; Cobley, C. M.; Zeng, J.; Li, W.; Moran, C. H.; Zhang, Q.; Qin, D.; Xia, Y. *Chem. Rev.* **2011**, *111*, 3669−3712.
(43) Kennedy, J. H.; Frese, K. W. *J. Electrochem. Soc.* **1978**, *125*, 709−714.
(44) Christopher, P.; Xin, H.; Linic, S. *Nat. Chem.* **2011**, *3*, 467−472.
(45) Rotenberg, N.; Bristow, A. D.; Pfeiffer, M.; Betz, M.; van Driel, H. M. *Phys. Rev. B* **2007**, *75*, 155426.
(46) Lakowicz, J. R. *Principles of Fluorescence Spectroscopy*, 3rd ed.; Springer Academic: New York, 2006.
(47) Li, M.; Wang, Q.; Shi, X.; Hornak, L. A.; Wu, N. Q. *Anal. Chem.* **2011**, *83*, 7061−7065.
(48) Singh, M. P.; Strouse, G. F. *J. Am. Chem. Soc.* **2010**, *132*, 9383−9391.
(49) Li, M.; Cushing, S. K.; Wang, Q.; Shi, X.; Hornak, L. A.; Hong, Z.; Wu, N. Q. *J. Phys. Chem. Lett.* **2011**, *2*, 2125−2129.
(50) Warren, S. C.; Thimsen, E. *Energy Environ. Sci.* **2012**, *5*, 5133−5146.
(51) Dressel, M.; Gruner, G. *Electrodynamics of Solids*; Cambridge University Press: Cambridge, 2002.
(52) Rzazewski, K.; Boyd, R. W. *J. Mod. Opt.* **2004**, *51*, 1137−1147.
(53) Kosuda, K. M.; Bingham, J. M.; Wustholz, K. L.; Van Duyne, R. *Compr. Nanosci. Technol.* **2011**, *3*, 263−301.
(54) Andrews, D. L. *Chem. Phys.* **1989**, *139*, 195−201.
(55) Jacak, J.; Krasnyj, J.; Jacak, W.; Gonczarek, R.; Chepok, A.; Jacak, L. *Phys. Rev. B* **2010**, *82*, 035418.
(56) Jung, J.; Trolle, M. L.; Pederson, K.; Pederson, T. G. *Phys. Rev. B* **2011**, *84*, 165447.